PHYSICAL REVIEW E **77**, 030801(R) (2008)

Conformation and trapping rate of DNA at a convergent stagnation point

Jennifer Kreft,[1,2] Yeng-Long Chen,[1,3,*] and Hsueh-Chia Chang[4]
[1]*Institute of Physics, Academia Sinica, Taipei, Taiwan*
[2]*Department of Chemistry, University of Texas at Tyler, Tyler, Texas 75799, USA*
[3]*Research Center for Applied Science, Academia Sinica, Taipei, Taiwan*
[4]*Chemical and Biomolecular Engineering, University of Notre Dame, Notre Dame, Indiana 46556, USA*
(Received 22 July 2007; published 5 March 2008)

We use a lattice-Boltzmann based Brownian dynamics simulation to investigate the elongation of DNA at a convergent stagnation point trapped by a uniform attractive potential. The trapping rate of the DNA is not sensitive to the potential and, consistent with a mean field theory, scales as the Peclet number, $Pe^{1/3}$. Surprisingly, we find that the coiled state is favored over the stretched state at high Pe. The final elongation is determined by conformation changes during transport to the stagnation point, rather than hydrodynamic stretching at that point.

DOI: 10.1103/PhysRevE.77.030801 PACS number(s): 61.25.H−, 83.50.Jf, 87.15.−v

Microfluidic technology is heralded as the future platform for biotechnology since it promises faster and less expensive medical diagnostics [1–3]. The design of these devices involves inventing novel methods for manipulating biopolymers such as DNA. A passive approach is to control fluid flow to manipulate the polymer position and conformation since viscous forces dominate in low Reynolds number microfluidic flow. For example, the position of a fluid drop in a four-roll mill device can be controlled by adjusting fluid impedence [4]. Using an analogous technique, the position of long polymers such as DNA at a junction can be controlled through fluid flow [5]. In optical mapping [6], the polymers are adsorbed and stretched on a surface by convective fluid flow. In addition, counter-rotating vortices have been used to deposit DNA precisely across electrodes [7] or concentrate bacteria [8–10] and are important in coffee-ring depositions [11,12,29].

Many of these techniques utilize a high shear rate flow near a stagnation point to trap and/or stretch DNA. However, the behavior of polymers in extensional flow can be complicated. Hysteresis in flow-induced polymer stretch was first theoretically predicted by de Gennes [13]. Recent experiments using long DNA molecules in extensional flow [5] or polystyrene in a filament stretching rheometer [14] have both shown that the coil-stretch transition is indeed hysteretic. Further simulations and theoretical studies have elucidated the importance of hydrodynamic interactions to the chain stretch hysteresis [15,16], as well as evidence of ergodicity breaking in the limit of infinite chain length [17]. In addition, the stretch-coil transition for elastic fibers has been theoretically examined and shown to be important in the motion of actin on myosin coated surfaces [18].

In this Rapid Communication, we study the trapping and steady state conformation of polymers in a stagnation region created by counter-rotating vortices. The polymers are trapped in the elongational flow by an attractive force along the top wall of the channel. We find that the conformation of a polymer as it enters the trap can be the primary factor determining the extension at the stagnation point for different shear rates.

We numerically simulated the counter-rotating vortices shown in Fig. 1 using the methods outlined in [19,20] based on the lattice-Boltzmann method. The fluid is coupled to a wormlike chain model with Brownian dynamics for the polymer [21,22]. The fluid velocity distribution function, $n_i(\mathbf{r},t)$, describes the fraction of fluid particles with a discretized velocity, $\mathbf{c_i}$, at each lattice site [23]. A three-dimensional, 19 discrete velocity scheme is used. The density ρ, momentum density $\mathbf{j}$, and momentum flux density $\mathbf{\Pi}$ are hydrodynamic moments of $n_i(\mathbf{r},t)$. At each time step, the velocity distributions will evolve according to

$$n_i(\mathbf{r}+\mathbf{c_i}\Delta\tau,t+\Delta\tau)=n_i(\mathbf{r},t)+\mathbf{L}_{ij}[n_j(\mathbf{r},t)-n_j^{eq}(\mathbf{r},t)], \quad (1)$$

where $\mathbf{L}$ is a collision operator such that the fluid relaxes to the equilibrium distribution. $\mathbf{L}$ has eigenvalues $\tau_0^{-1},\tau_1^{-1},\ldots,\tau_{18}^{-1}$, which are the characteristic relaxation time of the qth moment. We use the simple Bhatanagar-Gross-Krook model [24]: the nonconserved moments have a single relaxation time, $\tau_s=1.0$. Fluid stress fluctuations are added to the fluid as in the method of Ladd [23].

The 2-λ DNA used in the simulation is represented by a

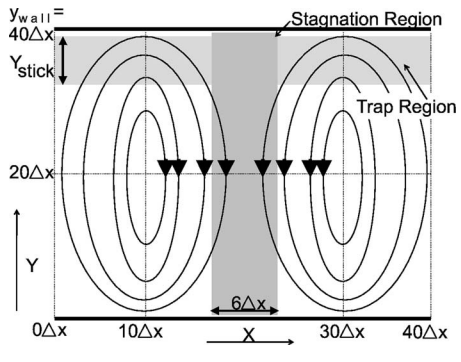

FIG. 1. Simulation setup, not to scale. Indicated are the region where the trapping force is active (trap region) and its width (Y_{stick}), and the region used to determine the trapping rate (stagnation region).

*Corresponding author. yenglong@phys.sinica.edu.tw

wormlike chain model parameterized to capture the dynamics of λ DNA in bulk solution at room temperature [25]. Each molecule is represented by $N_{bead}=22$ beads and $N_s=21$ springs with a contour length of 42 μm and radius of gyration of 1.06 μm. The forces acting on the bead include excluded volume effects, the elastic spring force, the viscous drag force, repulsion from the walls, and attraction to the top wall [19]. The fluid lattice size, Δx, is chosen to be 0.5 μm. The beads undergo Brownian motion with a Gaussian distribution with zero mean and a variance $\sigma_v=2k_BT\zeta\Delta t$, where k_B is Boltzmann's constant, T is the temperature, Δt is the time step, and $\zeta=6\pi\eta a$, where η is the viscosity of the fluid and a is the hydrodynamic radius of the bead. In this work, the number of polymers, N_p, is 25 unless otherwise noted, and the container size is $40\Delta x\times 40\Delta x\times 2\Delta x$. The time step for the fluid is $\Delta\tau=8.8\times10^{-5}$ s, and for the polymer $\Delta t=3.7\times10^{-6}$ s. The total simulation time is over ten chain relaxation times, allowing sufficient independent samples to perform statistical analysis. The chain relaxation time, $\tau_r=0.309$ s, is determined from the extensional relaxation time in the simulation.

Two counter-rotating vortices are produced by introducing external forces to the fluid bound by walls in the y direction and periodic in the x and z. Two forces of equal magnitude push on the fluid in the upper y region ($20\Delta x<y<40\Delta x$): one in the $+x$ direction along $x=10\Delta x$, and one in the $-x$ direction along $x=30\Delta x$. The beads are repelled from the walls with a force of magnitude:

$$F_{wall}=\frac{250k_BT}{\sigma_k^3(y_{bead}-y_{wall})^2},\quad y_{bead}>(y_{wall}-1),\qquad(2)$$

where the repulsion range is $1\Delta x$ and the Kuhn segment length is $\sigma_k=0.106$ μm. Each monomer will also be attracted to the top wall by a force with magnitude

$$F_{stick}=\frac{25K_{stick}k_BT}{\sigma_k^3(y_{bead}-y_{wall}+10)^2},\quad y_{bead}>(y_{wall}-Y_{stick})\qquad(3)$$

and range Y_{stick} (see Fig. 1). We vary both Y_{stick} and K_{stick} to test how the polymer dynamics depends on the attractive force and to mimic different attraction mechanisms.

Often, the Deborah number (the shear rate × the chain relaxation time) has been used to characterize chain stretching in flow [5,14,15,17,26]. However, it is difficult to define an appropriate shear rate for rotating vortices. We therefore define the Peclet number, Pe $u_{max}L/D_m$, where u_{max} is the maximum speed of the vortex, $L=40\Delta x$ is the box size, and D_m is the bead diffusion coefficient.

The polymers are initially carried by the convective flow and dispersed through the channel. Within a few seconds, the steady state configurations pictured in Fig. 2 are reached. We define the steady state as when the total number of beads in the trap region changes less than 5% over time. Three final configurations are possible: the "bundle" shown in Fig. 2(a), the "fountain" shown in Fig. 2(b), and the free configuration with polymers dispersed with the fluid flow (not shown). The free configuration occurs when the hydrodynamic drag forces overcome the trap force and the polymers follow the stream lines. As the vortex speed slows, all the beads on the chain become trapped in a bundle at the converging stagnation zone at the intersection of the trap and stagnation regions. In Fig. 2(a), some polymers are able to span the width of the channel due to the periodic boundary conditions. This configuration corresponds to one polymer being trapped in multiple stagnation zones and can be prevented by using polymers shorter than the box width. Finally, at slow vortex velocity, only parts of a chain become trapped, and polymers are stretched out of the stagnation zone into the vortices.

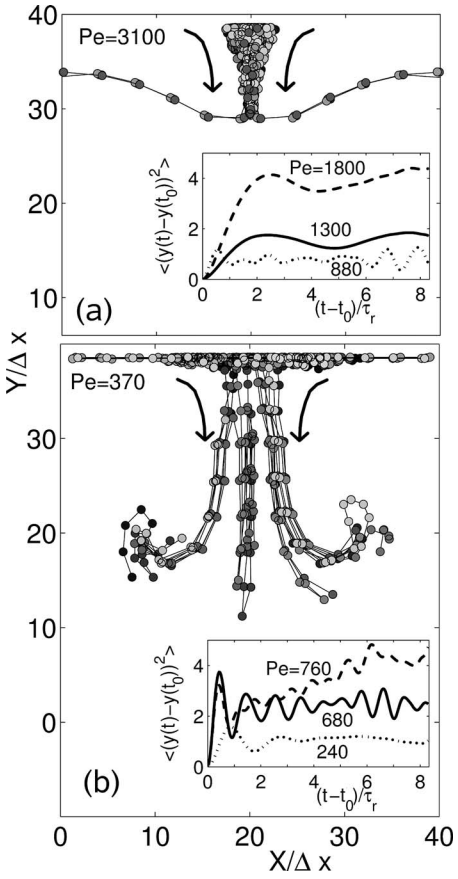

FIG. 2. Snapshot of the location of polymers for (a) Pe=3100 and (b) Pe=370 in the steady state. Arrows indicate the direction of fluid flow. Grayscale is used to indicate monomers of the same polymer. Insets: Mean square displacement in lattice units, Δx, of monomers in the (a) bundle and (b) fountain configuration. The time difference is normalized by τ_r. The error in the inset curves are of the order of the linewidth.

The mean square displacements of the beads indicates the transition from the freely flowing state to the bundle configuration (see insets of Fig. 2). Here, the mean square displacement is

$$\langle[y(t_0)-y(t)]^2\rangle=\frac{1}{N_{bead}}\sum_{i=1}^{N_{bead}}[y_i(t_0)-y_i(t)]^2,\qquad(4)$$

where t_0 is the time at which the steady state is reached. None of the beads, even at high Pe, move more than $5\Delta x$ from their original position within the time frame studied.

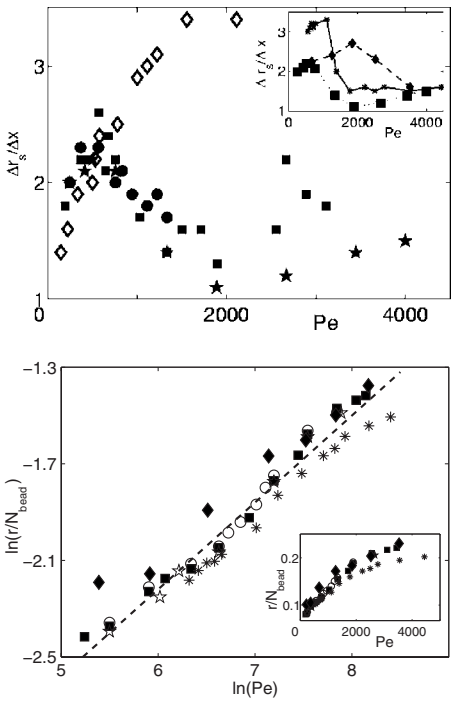

FIG. 3. Average spring extension Δr_s normalized by the lattice spacing Δx for different trapping conditions: $Y_{stick}=10\Delta x$ and circles (●): $K_{stick}=0.25$, squares (■): $K_{stick}=0.5$, stars (⋆): $K_{stick}=0.75$, and diamonds (◇): specific sticking force that acts only on the chain end. The inset shows results for different Y_{stick}: diamonds (◆): $Y_{stick}=1\Delta x$, $K_{stick}=0.75$, and $N_p=5$; asterisk (*): $Y_{stick}=5\Delta x$ and $K_{stick}=0.50$; and squares (■): $Y_{stick}=10\Delta x$ and $K_{stick}=0.50$. The error in average extension between data subsets (two sets of ten chains) is less than 5%. The extension of an individual polymer varies between 20% and 85% of the total chain length as the chain dynamics evolve in the flow.

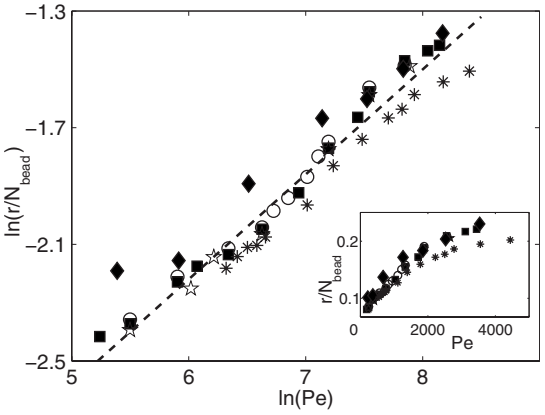

FIG. 4. Number of monomers trapped in the initial 8.8×10^{-2} s, r, normalized by the total number of monomers, N_{bead}, vs Pe on a log-log plot. Symbols are equivalent to those in Fig. 3. The dashed line has a slope of 0.36. The inset shows the same data on a linear plot.

Periodic motion is observed in the mean square displacement. At low Pe, the oscillations are due to the polymers' free ends rotating in the flow. The frequency is equal to that of the vortices and therefore increases with Pe. The transition between bundled and fountainlike configurations is clear as the mean square displacement decreases fourfold between Pe=760 and 880, although a significant number of polymers are extended at Pe=880. Near this transition some polymers may remain freely flowing in the steady state.

Above Pe=900, most of the polymers are trapped, but still rotate within the bundle. The polymers near the boundary of the stagnation are sheared by the vortices. The dynamics result from the balance between the attractive wall force, the chain entropic spring, and the shearing force of the flow. The monomers move toward the tip of the bundle, and the attractive trap and entropic spring force pulls them back to the wall. The period is many chain relaxation times and longer than that observed in the fountainlike state.

To compare with previous works on polymer stretching, we measure the average spring extension for different Peclet numbers. The spring extension is defined as

$$\Delta r_s = \frac{1}{N_s}\sum_{i=1}^{N_s} |r_i - r_{i+1}|, \tag{5}$$

where r_i is the position of bead i. As can be seen in Fig. 3, the chain extension first increases at low Pe, then decreases above a critical Pe (Pe_C). This is in sharp contrast with studies of chains in extensional flow where the chain extension increased as the pull on the polymers increased [5,13–15,17,26,27]. The nonmonotonic trend observed here results from the nonspecific trapping attraction, which hinders chain stretching near the top wall. For comparison, we also considered an end tethered chain, and the nonmonotonicity is absent, with the spring extension only increasing with Pe as shown in Fig. 3. For chains trapped in the bundled state, Δr_s again increases at Pe$>$2000 due to the shear force exerted on the beads at the outer edge of the bundle. Although the spring extension is only weakly dependent on K_{stick}, the extension depends strongly on the size of the trap, Y_{stick}, with Pe_C increasing as Y_{stick} decreases (see inset of Fig. 3).

To understand why increased flow leads to a decrease in extension, the dynamics of the polymers entering the trap must be understood. The contractional flow at the top wall compresses the polymer as it migrates toward the stagnation zone. A polymer of initial stretch l_0 contracted by a shear rate γ over the transit time τ will have length $l=l_0(1-\gamma\tau)$ when it reaches the stagnation zone. l/Y_{stick} thus determines whether the chains are in the bundled ($l/Y_{stick}<1$) or the fountain ($l/Y_{stick}>1$) state. The critical shear rate is $\gamma_C=(1-Y_{stick}/l_0)/\tau$. τ will be a weak function of Pe since the trapping segregates a monomer's trajectory from the streamline. Given $Pe=\gamma L^2/D_m$, Pe_C decreases with Y_{stick} as can be seen in the inset of Fig. 3.

Although the spring extension shows a dependence on Pe, the trapping rate is well-modeled by the classical mean-field convection-diffusion theory. We find a polymer depleted region near the trap boundary whose thickness decreases with Pe. This layer corresponds to the diffusion layer of the clas-

sical theory, which neglects both the polymer elastic force and bead-wall interactions [28]. Outside this layer, diffusion is unimportant compared to convection. Within the layer, normal diffusion becomes as significant as the tangential convection. Balancing these two fluxes for simple shear flow near the wall yields a $Pe^{-1/3}$ scaling for the thickness of the diffusion layer. The total polymer flux into the trap region is governed by the normal diffusive flux and scales inversely with the diffusion layer thickness. This predicted $Pe^{1/3}$ rate for high Pe convection enhanced trapping is in good agreement with the simulation results, as seen in Fig. 4. The best fit for different values of Y_{stick} and K_{stick} shows a $Pe^{0.36}$ dependence, indicating the trapping rate is independent of the bead-wall interaction. DNA trapping is a mass-transfer limited docking event.

We find that a nonspecific attractive force can be used to accumulate DNA at a convergent stagnation point. The polymers, if trapped, will take one of two configurations: "fountainlike" conformations at low Pe and "bundled" at high Pe. The nonintuitive observation that high vortex velocity leads to the coiled state is understood by investigating the dynamics of the polymer trapping. In prior works of chain stretching by extensional flow, the initial conformation of the polymer led to an increase in variability in final chain configurations [27]. A similar phenomenon is found here when a nonspecific trap force is included. The chain conformation as it enters the trap region determines the final state and extension of the polymer for all flow rates. Our simulations exhibit the scaling predicted by mean field theory for the diffusion layer thickness and trapping rate. These predictions provide insights into how the dynamics of long polymers in counter-rotating flow are important in evaporating droplets and applications utilizing convection.

We thank S. Maheshwari and X. Cheng for helpful discussions. J.K. and Y.L.C. were supported by the Li Foundation and Grant No. NSC 95-2112-M-001-051-MY3. H.C.C. was partially supported by a NSF grant.

[1] P. Yager, T. Edwards, E. Fu, K. Helton, K. Nelson, M. R. Tam, and B. H. Weigl, Nature (London) **442**, 412 (2006).
[2] R. G. Blazej, P. Kumaresan, and R. Mathies, Proc. Natl. Acad. Sci. U.S.A. **103**, 7240 (2006).
[3] H.-C. Chang, Can. J. Chem. Eng. **84**, 1 (2006).
[4] B. J. Bentley and L. G. Leal, J. Fluid Mech. **167**, 219 (1986).
[5] C. M. Schroeder, H. P. Babcock, E. S. G. Shaqfeh, and S. Chu, Science **301**, 1515 (2003).
[6] W. Wang, J. Lin, and D. C. Schwartz, Biophys. J. **75**, 513 (1998).
[7] H.-Y. Lin, L.-C. Tsai, P.-Y. Chi, and C.-D. Chen, Nanotechnology **16**, 2738 (2005).
[8] J. Wu, Y. Ben, D. Battigelli, and H.-C. Chang, Ind. Eng. Chem. Res. **44**, 2815 (2005).
[9] Z. Gagnon and H.-C. Chang, Electrophoresis **26**, 3725 (2005).
[10] D. Hou, M. Maheshwari, and H.-C. Chang, Biomicrofluidics **1**, 014016 (2007).
[11] H. Hu and R. G. Larson, J. Phys. Chem. B **110**, 7090 (2006).
[12] H. Hu and R. G. Larson, Langmuir **21**, 3963 (2005).
[13] P. G. deGennes, J. Chem. Phys. **60**, 5030 (1974).
[14] T. Sridhar, D. A. Nguyen, R. Prabhakar, and J. R. Prakash, Phys. Rev. Lett. **98**, 167801 (2007).
[15] C. M. Schroeder, R. E. Teixeira, E. S. Shaqfeh, and S. Chu, Macromolecules **38**, 1967 (2005).
[16] P. Sunthar and J. Ravi Prakash, Macromolecules **38**, 617 (2005).
[17] V. A. Beck and E. S. Shaqfeh, J. Chem. Phys. **124**, 094902 (2006).
[18] Y. N. Young and M. J. Shelley, Phys. Rev. Lett. **99**, 058303 (2007).
[19] Y.-L. Chen, H. Ma, M. D. Graham, and J. J. dePablo, Macromolecules **40**, 5978 (2007).
[20] J. Kreft and Y.-L. Chen, Phys. Rev. E **76**, 021912 (2007).
[21] P. Ahlrichs and B. Dünweg, J. Chem. Phys. **111**, 8225 (1999).
[22] P. Ahlrichs and B. Dünweg, Int. J. Mod. Phys. A **9**, 1429 (1998).
[23] A. J. C. Ladd, J. Fluid Mech. **271**, 285 (1994).
[24] P. Bhatnagar, E. P. Gross, and M. K. Krook, Phys. Rev. **94**, 511 (1954).
[25] R. M. Jendrejack, E. T. Dimalanta, D. C. Schwartz, M. D. Graham, and J. J. de Pablo, Phys. Rev. Lett. **91**, 038102 (2003).
[26] T. Perkins, D. Smith, and S. Chu, Science **276**, 2016 (1997).
[27] R. G. Larson, H. Hu, D. E. Smith, and S. Chu, J. Rheol. **43**, 267 (1999).
[28] L. G. Leal, *Laminar Flow and Convective Transport Process* (Butterworth-Heinemann, London, 1972).
[29] S. Maheshwari, L. Zhang, Y. Zhu, and H.-C. Chang, Phys. Rev. Lett. **100**, 044503 (2008).